International Journal on Robotics, Automation and Sciences

Noise Estimation for MRI Images with Revised Theory on Histograms of Second-order Derivatives

Wai Ti Chan*

***Abstract* - Previous research by the author in the use of histograms of second-order derivatives showed that the differences between pixels in MRI images can be determined without referring to the ground truth for the purpose of noise reduction. Yet, the results of the previous research also showed that the methodologies used could not prevent false positives and negatives. To address this problem, a technique has been developed to involve multiple conditions that utilize the statistics of the histograms and the circumstances of neighbours in the vicinity of a pixel. The confusion matrix for this method shows that the technique has marginal but consistent improvement across the noise levels that are tested, compared to prior methods.**

Keywords: Second-Order Derivatives, Histograms, Laplace Curves, MRI Images, Confusion Matrix, Noise Estimation

I. Introduction

This paper is preceded by four other previous works. These previous works are about the use of histograms of second-order derivatives of pixels within an image. The first to third works involved noise reduction and contrast enhancement [1][2][3]. The fourth work is also about noise reduction, with a method that improved on the previous ones [4].

The first to third works involve the use of only one Laplace curve. The methodologies in these previous works performed well for images that are heavily corrupted by noise. However, they do not perform as well for images that have relatively low noise. The results were some losses in detail, due to blurring caused by false positives. The fourth work involves the use of an additional curve. The results were better but were also affected by false positives as well as false positives.

Thus, there was the conclusion that any further development of methods that utilize the aforementioned histograms and Laplace curves must involve the use of confusion matrices to test for false negatives and positives.

II. Review of Previous Work & Additional Theories

The first to third works established the use of a Laplace curve that is generated using the statistical distribution of the second-order derivatives. The curve is compared with the histogram for differences in the shapes of their profiles. The analysis of the differences yields information that is useful for noise and contrast estimation [1][2][3].

The methodology of the fourth previous work uses an additional Laplace curve. This improves performance at higher noise levels, compared to methods with just one profile. This paper continues this hypothesis.

The fourth of the previous works also finds that the previous methods have been consistently effective at higher levels of noise. This is due to there being more

* Corresponding author. Email: wtchan@mmu.edu.my, ORCID: 0000-0002-2366-1851
Wai Ti Chan is with Faculty of Engineering and Technology (FET), Multimedia University (MMU), Jalan Ayer Keroh Lama, Bukit Beruang, 75450 Melaka, Malaysia. (Phone: +606-2523185; fax: +606 - 231 6552; e-mail: wtchan@mmu.edu.my).

International Journal on Robotics, Automation and Sciences (2023) 5,1:6-12
https://doi.org/10.33093/ijoras.2023.5.1.2
Manuscript received: 8 Dec 2022 | Revised: 20 Feb 2023 | Accepted: 27 Apr 2023 | Published: 30 Apr 2023

Published by MMU PRESS. URL: http://journals.mmupress.com/ijoras

pixels affected by noise, such that false positives and negatives become less of a concern [4]. This implied a need for the use of a confusion matrix.

To illustrate this need, data from the fourth of the previous works have been included in this paper as Figure 1 and Figure 2. The data in these charts is formed by comparing the results of processes with the algorithm that was developed in the previous works with the ground truth images [4].

In Figure 1, the first set of measuring criteria are the ratio of false positives to the number of pixels that have been selected for filtering and the ratio of false negatives to the number of pixels that have not been selected. In Figure 2, the second set of measuring criteria include the ratios of the false positives and negatives to the total number of pixels in the image. The ratios are in the form of percentages. The reasoning for this is that the sample images that are used have variable numbers of pixels. The ratios, in the form percentages, are appropriate for indicating the performance of a method when the sample images do not have fixed dimensions [5].

Figure 2 shows that the algorithm in the previous works does not do well at avoiding false negatives and positives at low levels of noise, whereas Figure 1 shows the algorithm having poorer performance at avoiding false negatives at higher noise levels.

The previous works considered the second-order derivative value of a pixel against the corresponding statistics from the histogram. The only other localized circumstance of a pixel that is utilized are the differences between the value of the pixel and those of its immediately adjacent neighbours [1]. The details of surrounding pixels that are further away, such as the population of pixels with similar values in the vicinity of the evaluated pixel, were not considered in previous works.

This omission, as revealed by the review of the previous works, gives rise to a theory. The theory is that pixels with similar second-order derivative values in the vicinity would contribute to any statistical method that is used to evaluate a pixel. This theory is based on the observation that there have been methods in which pixels are classified as being similar according to their values, such as the work done by Jeyalaksshmi & Prasanna in grouping pixels into regions according to their grayscale intensity [6].

III. METHODOLOGY

A. Sample MRI Images

The following methodology uses the same set of 150 MRI images as those used in previous works. The images came from sources such as Radiopaedia, The Cancer Imaging Archives (TCIA), Science Photo and National Library of Medicine.

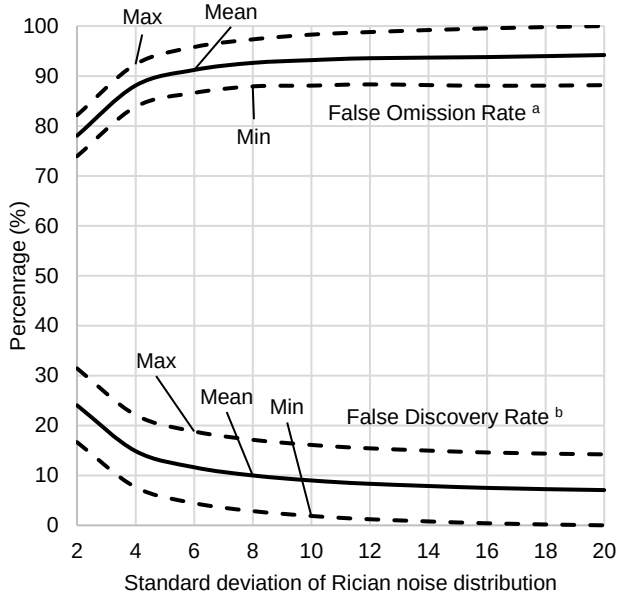

FIGURE 1. False omission and false discovery rates at different Rician noise levels, according to percentage of pixels selected and not selected, inclusive of variance; results of previous work.

a. This is the ratio of the number of pixels that have false positives to the number of pixels that have been selected for filtering, in percentage form.

b. This is the ratio of the number of pixels that have false negatives to the number of pixels that have not been selected for filtering, in percentage form.

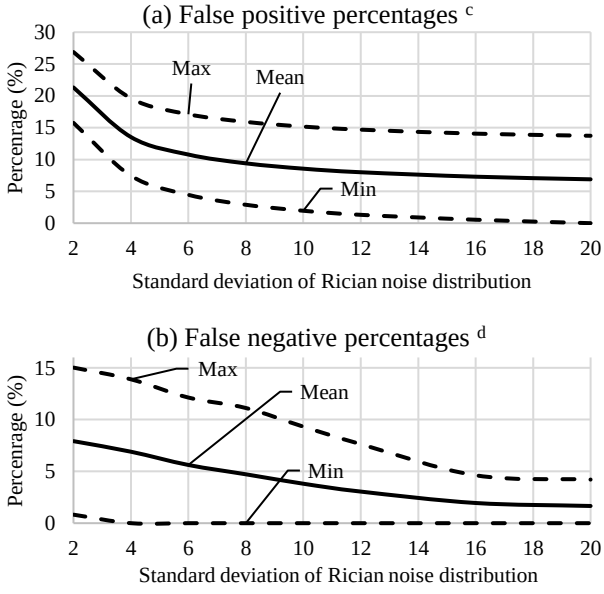

FIGURE 2. (a) False positive and (b) false negatives at different Rician noise levels, according to percentage of total number of pixels, inclusive of variance; results of previous work.

c. This is the ratio of the number of pixels that have false positives to the total number of pixels in an image, in percentage form.

d. This is the ratio of the number of pixels that have false negatives to the total number of pixels in an image, in percentage form.

The images have been selected for the variety in their image subjects, their dimensions and the presence (or lack thereof) of other details like text labels. In the previous works, these images have been useful for troubleshooting flaws in the algorithms and their responses to the diversity in the images. They are also useful for the work that is described in this paper.

B. Histograms of Second-Order Derivative Values

As in the previous works, the methodology in this paper retains the method of acquiring the second-order derivative values. This is achieved through the application of a 2D Laplacian operator with four masks. There is a 3 × 3 mask for each pixel that is away from the edges, a 3 × 2 mask for each pixel on the vertical edges, a 2 × 3 mask for each of those on the horizontal ones and a 2 × 2 mask used on each pixel in the corners [1][2]. The derivative values are then collated as a frequency histogram.

To avoid redundancy and any further self-citation, any further elaboration is omitted from this paper.

C. Laplace Curves on Histogram

As in past works, a Laplace curve is generated using the distribution of the second-order derivative values. This curve is then laid over the profile of the histogram for comparison [1][2]. The second and third of the previous works implement a second curve. The second curve is generated from the frequency interval for the second-order derivative value of zero. The details of this methodology can be examined in the article of the previous works [2][3].

As a summary of those previous works, the first curve is generated with σ_1, which is the standard deviation of the distribution of the second-order derivative values. The second curve is generated with σ_2, which is a standard deviation that is derived via a recursive process using (1) (which is an adaptation of the Laplace probability distribution function).

$$\sigma_2 = 2^{0.5} b$$
$$h(0) = N\left(\frac{1}{2b} exp\left(-\frac{|0-\mu|}{b}\right)\right) \qquad (1)$$

Where σ_2 is the standard deviation for the second curve,
$h(0)$ is the frequency of the second-order derivative value of zero in the histogram,
N is the number of pixels in the image, and
μ is the average of the second-order derivative values.

D. Ratios of Heights of Curves and Frequency Intervals to Total Number of Pixels

The previous works utilize the arithmetic differences between the frequency intervals in the histogram and the corresponding heights of first and second Laplace curve. There is a difference in the methodology that is described in this article compared to those in previous works. This methodology utilizes the ratios of the heights of the curves and the frequency intervals to the total number of pixels.

Each distinct second-order derivative value has three of these ratios. The ratios and their component quantities are defined as follows:

- j, distinct second-order derivative value
- $h_{1,j}$, height of the first Laplace curve at the point that corresponds to j
- $h_{2,j}$, height of the second Laplace curve at the point that corresponds to j
- N, total number of pixels in the image, mentioned earlier.
- R_1 , ratio of $h_{1,j}$ to N
- R_2 , ratio of $h_{2,j}$ to N

These ratios are considered global variables. This is because they are independent of the local circumstances of a pixel. The ratios are to be compared against a ratio that is determined with the local circumstances of the pixel. Comparing global variables to local ones has been documented as a method of image processing for the purpose of determining locations of interest [7]. This technique is applied here to further the theory that deviations from the statistics of the second-order histogram would reveal the presence of noise, as have been posited in previous works.

E. Ratio of Number of Pixels with Similar Second-Order Derivative Values to Number of Pixels in the Vicinity

The local circumstances of a pixel are represented by the other pixels around the pixel that is being evaluated. An 11 × 11 mask with the pixel at the center is applied to obtain a sampling of the other pixels in the vicinity. The mask is altered to accommodate pixels that are at the edges or corners of the images, like what is described in section B.

A ratio is derived from this sampling. The ratio and its component quantities are defined as follows:

- j, the second-order derivative value of the pixel being evaluated, corresponding to j as described previously.
- L , the total number of pixels within the mask
- L_j , number of pixels with value of j within the mask
- R_L , the ratio of L_j to L

F. Threshold Conditions

The ratio R_L is to be compared with ratios R_1 and R_2. This comparison is implemented as thresholds for a step that is described later. The comparison involves two thresholds, which are defined as follows:

- Condition #1: R_1 is less than R_L
- Condition #2: R_2 is less than R_L

If both conditions are fulfilled, the pixel is determined

as being affected by noise. Otherwise, the pixel is considered as not being affected by noise. The results of this determination are then compared with the ground truth images as per the procedures for a confusion matrix.

G. Confusion Matrix

The accuracy of the method is to be presented via the following ratios:

- Ratio of false positives to the sum of true positives and false positives, i.e. the false discovery rate; the sum is the number of pixels that the algorithm has determined as being affected by noise.
- Ratio of false negatives to the sum of true negatives and false negatives, i.e. the false omission rate; the sum is the number of pixels that the algorithm has determined as not being affected by noise.
- Ratio of false positives to the total number of pixels in the image; this is used to investigate the response of the algorithm to images of different sizes.
- Ratio of false negatives to the total number of pixels in the image; this has the same purpose as the above.

Incidentally, the ratios can be used to determine the response of a method to different scenarios [8]. In this case, the scenario is the increasing level of Rician noise that is introduced into the ground truth images.

H. Goal of Testing

Ideally, the results should be better than the ones shown in Figure 1 and Figure 2. In particular, the false discovery rates at low levels of noise should be lower and the false omission rates at high levels of noise should be lower too. The ratios from the results of this methodology that correspond to those in Figure 2 should also be more consistent, i.e., the variance is less.

IV. RESULTS & DISCUSSION

A. Example of Implementation of Termination Factor

Figure 3 shows an example of the sample MRI images. This one has been included due to the presence of various distinct viscera. The distinct viscera test the methodology on how it can differentiate regions. This image has been corrupted with Rician noise at a standard deviation of distribution of 2.

The confusion matrix for this is as shown in Table I. As can be observed, the percentage of false positives is significant for this image. This is because small and distinct details are interpreted as noise by the algorithm in this method. Incidentally, this finding also occurred in previous works. Thus, the methodology that is described in this paper has not addressed this setback.

FIGURE 3. Abdominal MRI image of a woman, 47 days after giving birth; image source: National Library of Medicine.

TABLE 1. False positives and false negatives for the image in Fig. 1 in terms of percentages of pixels in the image.

Condition	Positive	Negative
True	80.43%	0.19%
False	18.67%	0.71%

B. Results of Tests on Sample MRI Images

Figure 4 and Figure 5 show the results of the testing with the sample images. Compared to Figure 1, Figure 4 shows marginal improvements for the false discovery rates, i.e., reductions in the percentages, across the noise levels. The reason for this is implied in the differences in the false omission rates between the two pairs of charts.

The false omission rates are marginally lower for both averages and standard deviations at low to middle levels of noise, e.g., standard deviation of 2 to 8. This implies that the methodology that is used in this research has selected more pixels that are affected by noise, but only incrementally. However, the variance of the rates is narrower in Figure 1 than in Figure 4.

At high levels of noise, e.g. beyond standard deviation of 12, the methodology that is used selects almost all pixels. Yet, this did not lead to high false omission rates. Instead, there are false omission rates of zero for these levels. The false discovery rates at these levels of noise are also marginally lower, thus suggesting an overall small improvement.

Figure 5(a) shows false positives that are slightly higher across noise levels, thus suggesting a less discriminate selection of pixels. However, this is compensated for by a significant reduction in false negatives. In particular, the false omission rates converge to zero at noise levels of beyond standard deviation of 12.

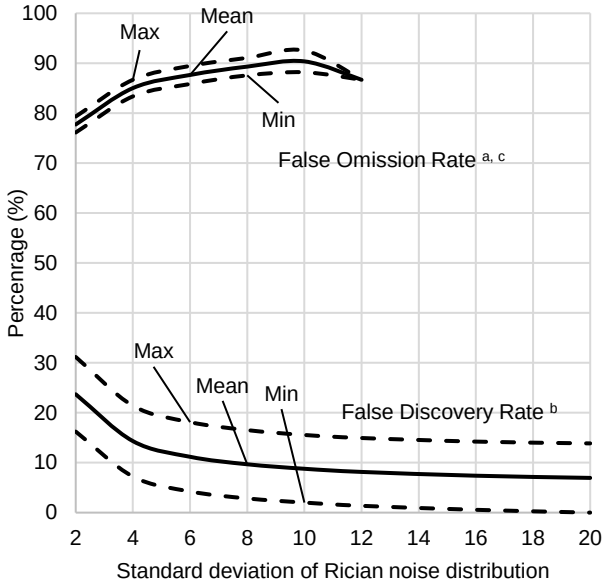

FIGURE 4. False omission and false discovery rates, according to Rician noise level and percentage of pixels selected and not selected, inclusive of variance; results of current work.

a. This ratio is the number of pixels that have false positives to the number of pixels that have been selected for filtering, in percentage form.

b. This ratio is the number of pixels that have false negatives to the number of pixels that have not been selected for filtering, in percentage form.

c. The rates for standard deviations beyond 12 are zero; they have been omitted for better display of the results.

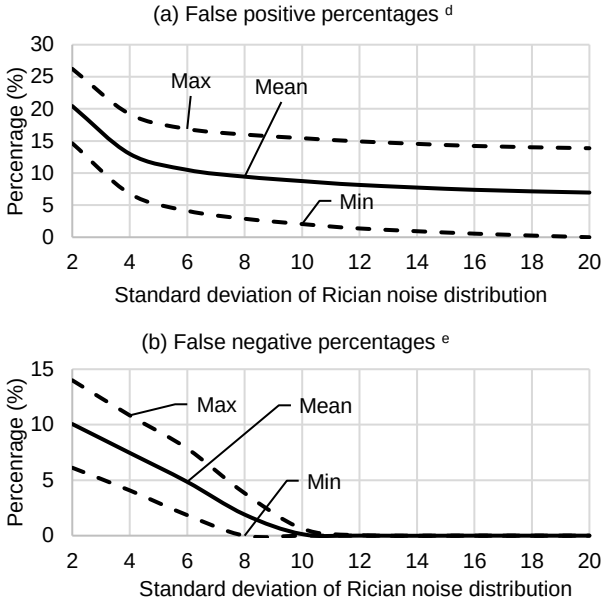

FIGURE 5. (a) False positive and (b) false negatives, according to Rician noise level and percentage of total number of pixels, inclusive of variance; results of current work.

d. This ratio is the number of pixels that have false positives to the total number of pixels in an image, in percentage form.

e. This ratio is the number of pixels that have false negatives to the total number of pixels in an image, in percentage form.

C. Prior Algorithms

Before this research work settled on the use of the algorithm as described in the Methodology section, there were previous versions of the algorithm with lesser results.

In particular, one of these previous versions uses the arithmetic differences between the frequency intervals in the histogram and the corresponding heights of the Laplace curves, as per the methodologies of previous works. These have poorer performance than the algorithm that is described here. The results of this version of the algorithm are not shown here to avoid redundancy.

Thus, the theory that is based on these arithmetic differences has to be revised [3][4]. The results that are shown in Figure 4 and Figure 5, when compared to those in Figure 1 and Figure 2, further contribute to this finding.

D. Notable Anomalies for Results with MRI Scans of Vascular Complications

The 150 sample images include MRI scans of vascular complications, such as the scan of a cerebral arteriovenous malformation as shown in Figure 6. The results for these images consistently register a false omission rate of zero at low levels of noise. There is no notable trend in the false discovery rates.

This is likely due to the setting of the scans, having been calibrated for the detection of vascular objects, e.g., blood vessels and capillaries, which appear as grainy regions in the images. In previous works with methods that utilize histograms of second-order derivatives, the algorithms would register these as noise [1]. In the case of the algorithm that is used in this methodology, more pixels in these images are selected than in other images. However, the false discovery rates are not significantly worse, which suggests that this is not a flaw in the algorithm.

FIGURE 6. MRI image of arteriovenous malformation in cerebrum; image source: National Library of Medicine.

E. Comparison with Other Works

The benchmarking of the methodology in this research depends on the following characteristics:

- MRI images with Rician noise.
- Usage of convolution methods to determine the presence of noise, pixel by pixel.
- Usage of confusion matrices to verify results.

The literature review did not yield any other research with a methodology that strictly matches all the characteristics. However, there were two that are partially comparable to the research in this paper.

Manjón & Coupé worked on a technique that uses convolution-based method for MRI images with Rician noise [9]. However, qualitative evaluation was used for the results, i.e., the resulting images were visually compared to the real ones, so confusion matrices were not used. On the other hand, Table 5 in the cited paper does show a table of PSNR scores [9]. Although the image sets that were used are different from those in this research and previous works, the results have a similar trend to that in previous works [2][3]; this trend is a general reduction in PSNR scores as overall noise level increases. Thus, it can be inferred that the technique described by Manjón & Coupé does not address the issue of false positives and negatives.

M. Fayaz et al. developed a methodology to classify MRI images with statistical calculations. It includes noise removal with morphological techniques. The results are checked with a confusion matrix [10]. The methodology of M. Fayaz et al. does not apply the confusion matrix on a pixel-by-pixel basis, unlike what is done here. On the other hand, they applied additional steps, e.g., the conversion of grayscale images to RGB, to overcome limitations in previous methods; this is similar to what is done in this paper. However, the improvement in their results was marginal, e.g., 1.3% over the most recent previous method, according to accuracy tests that have been implemented across their previous methods; this is like the findings of this research. Although the confusion matrices that are used for their methods are not directly comparable to the one described here, the similarity of marginal improvement over previous methods is notable.

V. CONCLUSION & RECOMMENDATION

The algorithm in the methodology of this paper does not give a substantial improvement at avoiding false positives and negatives. The improvement is only marginal, when compared to the earlier methods that utilize second-order histograms.

On the other hand, the improvements are consistent throughout the noise levels, e.g., the methodology in this paper is more reliable at selecting pixels that are affected by noise. This improvement is due to the introduction of another condition that also makes use of the second-order derivatives of pixels. Instead of a distribution-based condition, such as the frequency histograms that are in previous works, this condition is based on the circumstances of neighbouring pixels. Thus, having more and different conditions for the determination of noise-affected pixels is feasible for improving performance.

The aforementioned anomaly of virtually zero false omission rates for MRI images of vascular objects is notable. This finding suggests that there is practical application in further developing this algorithm into a diagnostic tool. This would involve tests with MRI scans of the blood vessels of healthy subjects and subjects with vascular problems, in order to test the reliability of such an algorithm.

However, expectations of improvement would have to be kept modest. The findings of this research and other similar research suggest that increasing complexity in methodology does not yield proportional improvement in accuracy.

ACKNOWLEDGMENT

We thank the anonymous reviewers for the careful review of our manuscript.

FUNDING STATEMENT

There is no financial support from any agencies funding this research work.

AUTHOR CONTRIBUTIONS

Wai Ti Chan: Conceptualization, Data Curation, Methodology, Validation, Writing – Original Draft Preparation;

CONFLICT OF INTERESTS

No conflict of interests were disclosed.

ETHICS STATEMENTS

Our publication ethics follow The Committee of Publication Ethics (COPE) guideline. https://publicationethics.org/

REFERENCES

[1] W.T. Chan, K.S. Sim, and F.S. Abas, "Contrast Measurement with Histograms of Second-order Derivatives of Pixels for Magnetic Resonance Images," *Engineering Letters*, vol. 27, no. 2, pp. 390–395, 2019.
URL: https://www.engineeringletters.com/issues_v27/issue_2/EL_27_2_16.pdf

[2] W.T. Chan, K.S. Sim, and F.S. Abas, "Pixel Filtering and Reallocation with Histograms of Second-order Derivatives of Pixel Values for Electron Microscope Images," *International Journal of Innovative Computing Information and Control*, vol. 14, no. 3, pp. 915–928, 2018.
DOI: https://doi.org/10.24507/ijicic.14.03.915

[3] W.T. Chan and K.S. Sim, "Termination Factor for Iterative Noise Reduction in MRI Images Using Histograms of Second-order Derivatives," *IAENG International Journal of Computer Science*, vol. 48, no. 1, pp. 174–180, 2021.
DOI: https://www.iaeng.org/IJCS/issues_v48/issue_1/IJCS_48_1_19.pdf

[4] W.T. Chan, "Conditional Noise Filter for MRI Images with Revised Theory on Second-order Histograms," *International Journal on Robotics, Automation and Sciences*, vol. 3, pp. 25–32, 2021.
DOI: https://doi.org/10.33093/ijoras.2021.3.5

[5] A. Tharwat, "Classification Assessment Methods," *Applied Computing and Informatics*, vol. 17, no. 1, pp. 168–192, 2018.
DOI: https://doi.org/10.1016/J.ACI.2018.08.003

[6] S. Jeyalaksshmi and S. Prasanna, "Measuring Distinct Regions of Grayscale Image Using Pixel Values," *International Journal of Engineering and Technology,* vol. 7, no. 1.1, pp. 121–124, 2018.
DOI: https://doi.org/10.14419/IJET.V7I1.1.9210

[7] V. Lakshmanan, "Global and Local Image Statistics," *Automating the Analysis of Spatial Grids*, Springer, pp. 91-128, 2012.
DOI: https://doi.org/10.1007/978-94-007-4075-4_4

[8] S.M. Boca and J.T. Leek, "A Direct Approach to Estimating False Discovery Rates Conditional on Covariates," *PeerJ*, vol. 6, no. e6035, 2018.
DOI: https://doi.org/10.1101/035675

[9] J.V. Manjón and P. Coupé, "MRI Denoising Using Deep Learning," *International Workshop on Patch-based Techniques in Medical Imaging*, pp. 12-19, 2018.
DOI: https://doi.org/10.1007/978-3-030-00500-9_2

[10] M. Fayaz, J. Haider, M.B. Qureshi, M.S. Qureshi, S. Habib, and J. Gwak, "An Effective Classification Methodology for Brain MRI Classification Based on Statistical Features, DWT and Blended ANN," *IEEE Access*, vol. 9, pp. 159146–159159, 2021.
DOI: https://doi.org/10.1109/ACCESS.2021.3132159